

# First detection of hotspot advance in a Compact Symmetric Object

## Evidence for a class of very young extragalactic radio sources

I. Owsianik<sup>1</sup> and J.E. Conway<sup>2</sup>

<sup>1</sup> Toruń Centre for Astronomy, Radio Astronomy Department, ul.Gagarina 11, PL-87-100 Toruń, Poland (iza@astro.uni.torun.pl)

<sup>2</sup> Onsala Space Observatory, S-439 92 Onsala, Sweden (jconway@oso.chalmers.se)

Received 2 December 1997 / Accepted 21 April 1998

**Abstract.** We present the results of multi-epoch global VLBI observations of the Compact Symmetric Object (CSO), 0710+439 at 5 GHz. Analysis of data spread over 13 years shows strong evidence for an increase in the separation of the outer components at a rate of  $0.251 \pm 0.029 h^{-1} c$ . Dividing the overall size of  $86.8 h^{-1} \text{pc}$  by this separation rate implies an estimated kinematic age of only  $1100 \pm 100$  yrs. After taking into account possible temporal variations in hotspot advance speeds due to cloud collisions or hydrodynamic instabilities we argue that the upper limit to the age of 0710+439 is most likely within a factor of 2 of this estimate and certainly within a factor of 10 (i.e.  $< 11\,000$  yrs). This result therefore strongly supports the idea that Compact Symmetric Objects are very young radio-loud sources. Furthermore the large radiative efficiency we calculate for 0710+439 is consistent with strong negative luminosity evolution as CSOs grow in size and with them evolving into classical double sources.

**Key words:** radio continuum: galaxies – galaxies: active – galaxies: compact – galaxies: evolution – galaxies: individual: 0710+439

### 1. Introduction

Most strong, compact ( $< 1''$ ) radio sources when imaged at high resolution have a core-jet morphology, consisting of a bright unresolved core and a one-sided jet in which superluminal motion is often observed. These core-jet sources are thought to be due to the bases of relativistically beamed jets orientated close to the line of sight. However Phillips & Mutel (1982) first identified compact objects which appeared to be dominated by two un-beamed emission components and called them ‘Compact Doubles’. Conway et al. (1992) described two similar objects with more complex triple structures. Given this wider range of morphologies Wilkinson et al. (1994) renamed this whole class of radio sources as ‘Compact Symmetric Objects’ (CSOs) emphasising their primary property of symmetry. Characteristically these objects show high luminosity radio emission regions separated by  $< 1 \text{kpc}$  which are located symmetrically on both sides

of the centre of activity. It is thought that these high brightness regions are due to hotspots and minilobes created by the termination of oppositely directed jets and that this emission is free from relativistic beaming effects. For a recent review of the properties of CSOs and related sources see O’Dea (1998).

From the earliest papers it was suggested that CSOs were young sources (Phillips & Mutel 1982), which evolved into larger-sized objects. Alternatively it has been proposed that CSOs are ‘frustrated’ sources, in which higher density and/or turbulence in the interstellar medium inhibits their growth to larger dimensions (van Breugel et al. 1984). Finally it has been proposed that they are a separate class of short lived objects, which ‘fizzle out’ after about  $10^4$  yrs and do not grow to large sized objects (Readhead et al. 1994).

Detailed theories of the youth model of compact sources show that it is feasible that CSOs are part of an evolutionary sequence in which they later evolve into the slightly larger Compact Steep Spectrum (CSS) sources, which finally evolve into classical doubles (Fanti et al. 1995, Readhead et al. 1996a,b). De Young (1996) and Begelman (1996) have used simple physical models to confirm that CSO sources are probably not frustrated and confined but instead evolving. An obvious way to distinguish between competing models is to try to measure or set limits on the growth in overall size of CSOs and so determine their ages directly, which is the purpose of this paper.

### 2. General source properties

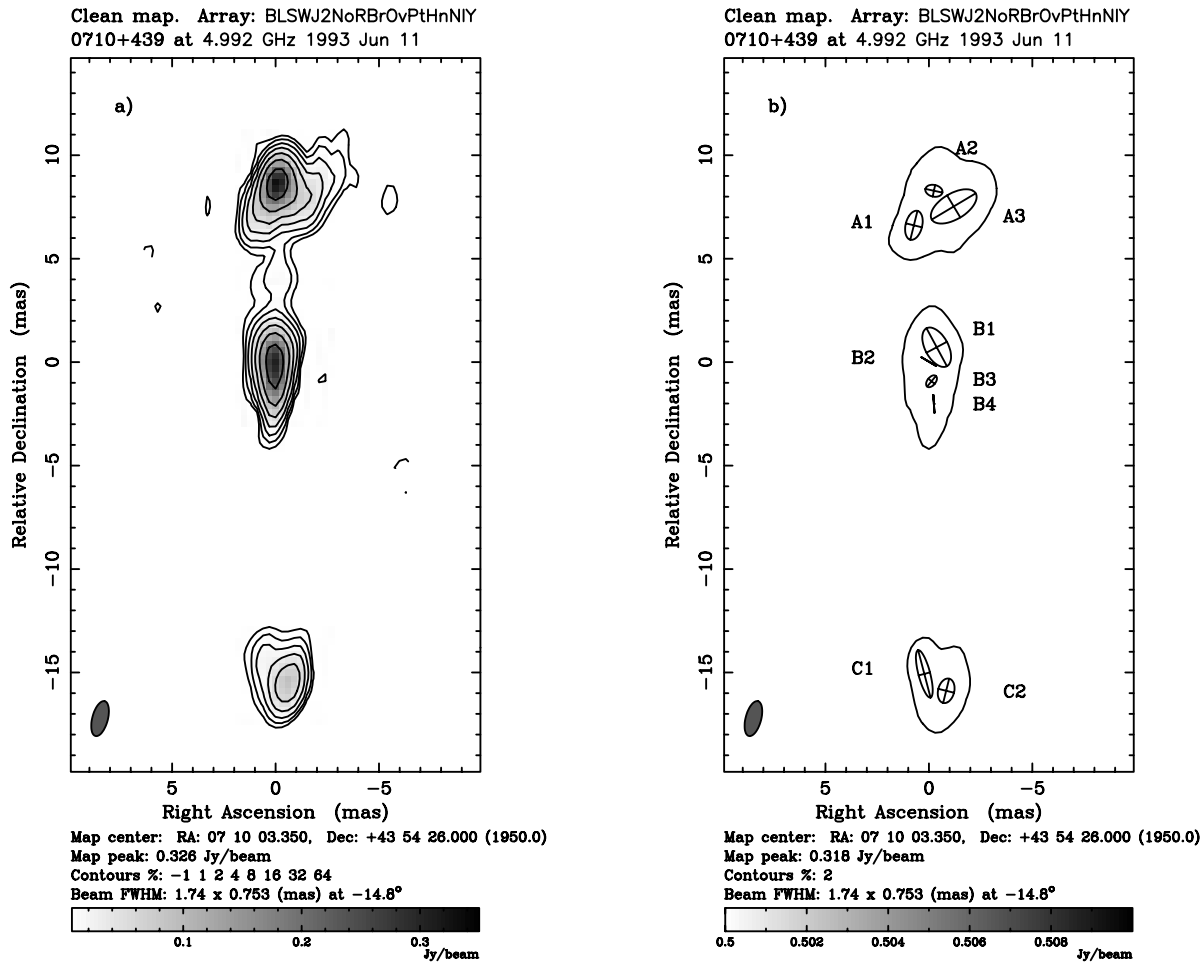
#### 2.1. Optical properties

The radio source 0710+439 has been identified (Peacock et al. 1981) with a galaxy of  $r$  magnitude of  $19.7 \pm 0.2$ . The emission-line redshift of the galaxy is  $z = 0.518$  (Lawrence et al. 1996). At this redshift  $1 \text{mas} = 3.6 h^{-1} \text{pc}$  assuming  $H_0 = 100 h \text{km s}^{-1} \text{Mpc}^{-1}$  and  $q_0 = 0.5$ . The optical spectrum (Lawrence et al. 1996) shows absorption lines characteristic of an evolved stellar population and an optical continuum shape typical of an elliptical galaxy without any evidence for a nonstellar component.

**Table 1.** Summary of 5 GHz global VLBI observations of 0710+439

Epoch	1980.53	1982.93	1986.89	1989.73	1993.44
Duration (hr)	11	12	4 × 1	10	4 × 0.6
Antennas <sup>a</sup>	BKGFo	BKGFo	SjBWKGFYo	SBWjKGFpKY	BLSWjNgROPHIY
Maximum baseline (Mλ)	136	136	136	138	146

<sup>a</sup> S—26 m, Onsala Space Observatory, Onsala, Sweden; j—26 m, MkII Telescope, Jodrell Bank, Cheshire, U.K.; B—100 m, Max-Planck-Institute für Radioastronomie, Effelsberg, Germany; W—Westerbork Synthesis Radio Telescope, the Netherlands; K—36.6 m, Haystack Observatory of the Northeast Radio Observatory Corporation, Westford, MA; G—42.7 m, National Radio Astronomy Observatory, Green Bank, WV; F—26 m, George R. Agassiz Station of Harvard University, Fort Davis, TX; Y—26 m, VLA, Socorro, NM; o—40 m, Owens Valley Radio Observatory of the California Institute of Technology, Big Pine, CA; L—32 m, Istituto di Radioastronomia, Medicina, Italy; N—32 m, Istituto di Radioastronomia, Noto, Italy; g—22 m, Simeiz, Ukraine; k—25 m, VLBA antenna, Kitt Peak, AZ; R—25 m, VLBA antenna, Brewster, WA; O—25 m, VLBA antenna, Owens Valley, CA; P—25 m, VLBA antenna, Pie Town, NM; H—25 m, VLBA antenna, Hancock, NH; I—25 m, VLBA antenna, N. Liberty, IA

**Fig. 1.** **a** Fifth epoch map of 0710+439. **b** Diagram with positions and sizes of the Gaussian model fit components

## 2.2. Radio properties

0710+439 has high radio luminosity ( $L_{5\text{GHz}} = 5 \times 10^{33} h^{-2} \text{ erg s}^{-1} \text{ Hz}^{-1}$ ; Wilkinson et al. 1994). The flux density is very weakly polarised ( $< 0.15\% \pm 0.11\%$  at 5 GHz) and the observed variations of the flux are not statistically significant (Aller et al. 1992). The total angular size of the source is 24.1 mas,

which corresponds to a projected linear size of  $86.8 h^{-1} \text{ pc}$ . The source has been mapped by VLBI at several frequencies i.e. 1.6, 5, 10.7, and 15 GHz. These observations showed the overall triple structure of the source. Despite having three components this source was provisionally classified as a compact double based on the fact that more than 80% of the emission

came from two almost equally bright components (Pearson & Readhead 1988). Conway et al. (1992) argued that the two outer components were hotspots and minilobes, while the centre of activity was associated with the middle component, based on its compactness, spectrum and weak flux density variability. Recent multi-frequency observations (Taylor et al. 1996) reveal a compact component with a strongly inverted spectrum at the southern end of the middle component, suggesting that the true centre of activity lies there.

### 3. Observations and imaging

#### 3.1. Observations

While at most frequencies 0710+439 has only been observed once, at 5 GHz it has been observed with a global VLBI array at 5 epochs spread fairly evenly over a period of 13 years (see Table 1). The first three epochs were analysed by Conway et al. (1992). Here we reanalyse these first three epochs and add new data from two additional epochs; a global 10 station long track observation made on 25th September 1989 and a multi-snapshot 13 station global observation made on 11th June 1993.

#### 3.2. Data reduction

Observations in all epochs were made in left circular polarisation (IEEE convention) and a bandwidth of 2 MHz was recorded using the MkII recording system (Clark 1973). The data were cross-correlated with the JPL-Caltech VLBI Processor. The data were fringe-fitted in AIPS (Schwab & Cotton 1983) and averaged to 1 minute; error bars for the averaged data were estimated from the internal scatter of the data over the averaging interval. Amplitude calibration for each antenna was derived from measurements of the antenna gain and system temperature during the observations.

After amplitude calibration the data were edited and mapped using IMAGR (AIPS package 1995) and Difmap (Shepherd et al. 1995). Many iterations of phase self-calibration were performed before applying amplitude self-calibration at the end. Windows for clean components were added to provide support and reject sidelobes. Initially each epoch was mapped separately starting with a point source model. The fitted restoring beams at each epoch were typically 1 mas in the East-West direction and 1.5 mas in the North-South direction. The highest dynamic range image was obtained from the 5th epoch data set (see Fig. 1a). Given this best map we therefore remade maps at all epochs using it as the starting model for self-calibration. As described in a Sect. 4 we then used these images to detect or set limits on internal motions within 0710+439.

Modelfitting with gaussian components was also carried out to the visibility data at each epoch using the program MODELFIT in the Caltech VLBI package (Pearson 1991), which fits to the amplitudes and closure phases directly, and also with the gaussian modelfitting option within Difmap. The latter fits amplitudes and phases but allows phase self-calibration against the model, so that the model can converge to fit the closure phases.

In all cases it was possible to obtain good fits to the data using only a few Gaussian components. The modelfitting process was started using gaussian components fitted to the 5th epoch CLEAN map using the AIPS task JMFIT. After varying all the gaussian parameters the best fitting model to the fifth epoch data contained 9 components (see Fig. 1b, Table 2). This model provided a good fit with reduced Chi-squared agreement factor for amplitude  $Q_{AMP}=1.258$  and for closure-phases  $Q_{CLP}=1.180$  (for definition of agreement factor see Henstock et al. 1995). To characterise temporal changes in the source we obtained fits to the data at each epoch, using this 5th epoch model as a starting point (see Sect. 4.1).

#### 3.3. Source structure

The CLEAN map of the 5th epoch data (rms noise = 0.9 mJy beam<sup>-1</sup>) shows clearly the overall triple structure of the source (see Fig. 1a). Maps at each epoch show three main components which we name (from North to South) A, B and C. Each of these main components shows substructure which is represented in the modelfits as separate gaussians (e.g. A1, A2 and A3; see Fig. 1b).

The CLEAN maps show that the northern (A) and the southern (C) components show some faint extended emission around them. In addition to this both modelfitting and imaging indicate a compact feature (A2) within component A which we interpret (see Sect. 5.1) as a hotspot. The CLEAN images suggest a weak bridge of emission between A and the middle component B, however imaging simulations show that this feature may not be reliable (see Appendix). We were not able to detect a similar jet-like feature connecting the middle and southern components, which was found on a 1.6 GHz map (Xu 1994), possibly due to lack of surface brightness sensitivity. We were also not able to detect any emission located to the East of the C component, which is seen on the maps made by Wilkinson et al. (1994).

Fitting the B component required 4 gaussian subcomponents. Fig. 2a,b show these gaussians as fitted to the 1st and 5th epochs respectively (convolved with a circular restoring beam of FWHM 0.7 mas). These images show that the B component is narrow at the South and becomes wider to the North. There also appears to be a slight kink in the jet with the major axis of the B3 component inclined at 45° with respect to the B2-B4 direction. A similar kink is seen in the 15 GHz maps and models (Taylor et al. 1996). Despite being separated by almost 13 years the model components for all 5 epochs are very similar. One possible change is in the size of B1, however we conclude based on our imaging simulations that this may be an imaging artifact. In Sect. 4 we describe our detailed analysis of the multi-epoch data which shows components B2 and B4 to be stationary relative to each other, with a possible small northward motion of B3.

Overall our maps and modelfits to B agree closely with those estimated at 15 GHz by Taylor et al. (1996). However in our modelfits we did not require a compact component at the position of the core seen at 15 GHz. This is not unexpected given that at high frequency this component has a self-absorbed spectral

**Table 2.** Model for the 5th epoch of 0710+439

Component	S (Jy)	r (mas)	$\Theta$ ( $^\circ$ )	a (mas)	b/a	$\Phi$ ( $^\circ$ )
A1...	0.069	6.654	6.261	1.439	0.556	-13.980
A2...	0.478	8.287	-1.670	0.840	0.675	77.764
A3...	0.251	7.623	-9.046	2.472	0.504	120.877
B1...	0.093	0.814	-27.553	2.081	0.537	28.275
B2...	0.274	0.028	15.555	0.831	0.003	59.254
B3...	0.214	0.932	-172.195	0.669	0.595	-39.600
B4...	0.144	2.033	-173.202	0.878	0.000	3.603
C1...	0.049	15.070	179.154	2.370	0.239	14.660
C2...	0.153	15.907	-176.993	1.210	0.645	166.070

Parameters of the Gaussian components: S—flux density; r, $\Theta$ —polar coordinates, with polar angle measured from the North through East; a,b—major and minor axes of the FWHM contour;  $\Phi$ —position angle of the major axis measured from the North through East

index of  $\alpha_{15\text{GHz}}^{8.4\text{GHz}} = 1.6 \pm 0.4$  (Taylor et al. 1996), where flux density  $S \propto \nu^\alpha$ . At 4.9 GHz with this spectral index we would expect the core to have a flux density of between 4.8 mJy and 11.8 mJy. At the position of the 15 GHz core on a 5th epoch super-resolved map (0.5 mas FWHM, not shown) we did see a component with flux density  $4.3 \pm 1$  mJy, if this feature is real it implies a spectral index of  $2.1 \pm 0.2$  between 4.9 GHz and 15 GHz consistent with a synchrotron self-absorbed spectrum core component.

## 4. Multi-epoch intercomparison

### 4.1. Procedure

A serious problem with analysing data from VLBI observations is that there is significant freedom in making images. Data are degraded by instrumental errors, incomplete and different aperture coverages, and ambiguities in deconvolution and self-calibration, all of which can strongly affect the final results. For this reason intercomparison of models and maps made separately at each epoch is not a good method of detecting small changes in a source (Conway et al. 1992).

To minimise the above effects we used the 5th epoch model and CLEAN map (see Fig. 1a,b) as starting points in re-modelfitting and re-mapping all of the epochs. This method should limit the differences between the final images of all five epochs of 0710+439, so we can be sure that any differences seen are demanded by the data and are due to real changes in the structure of the source (see Appendix).

The detailed procedure in modelfitting at each epoch was, starting with the 5th epoch model, to first allow just the flux density of all components to vary; however in each case the fit remained poor. We next allowed changes of all parameters of the gaussians within the B component (e.g. flux, radius,  $\Theta$ , major axis, axis ratio, and  $\Phi$ ) which gave a somewhat better fit, but only after allowing all the components to move in position (which led to significant motion mainly in component A2) did we get a good fit. Finally the  $u$ - $v$  data were amplitude self-calibrated against the model and one final iteration of modelfitting carried

out in which component positions were again allowed to vary. We note that it was never necessary at any epoch to change the size or shape of the gaussians within the A or C components. The final models had good agreement factors to the data (for epochs 1 to 5 total agreement factors were  $Q_{TOT}=1.149$ ,  $Q_{TOT}=1.047$ ,  $Q_{TOT}=1.039$ ,  $Q_{TOT}=1.145$  and  $Q_{TOT}=1.224$  respectively).

### 4.2. Component position and flux variations

From the modelfits we measured the separation of many pairs of components as a function of time and fitted linear regression lines to this data to estimate relative velocities (see Table 3, Fig. 3).

Although in VLBI data analysis various attempts have been made to estimate *a priori* error bars on component positions these schemes are of doubtful reliability. Gaussian error bars estimated from the variability of reduced Chi-squared on moving the components critically depend on the number of degrees of freedom in the data which depends in turn on the unknown degree of correlation of phase and amplitude errors with time. In addition as noted in Sect. 4.1 even our best fitting model has a reduced Chi-squared which is much further from unity than would be expected given statistical arguments. Given this situation we chose instead to estimate errors on motions from the internal scatter of our separation versus time data using standard methods of linear regression analysis. These methods applied to our data suggest that for the brighter components the random errors on the relative separation in each epoch are of order  $20\mu\text{as}$ . This is comparable to the estimates we obtained from imaging simulations (see Appendix A.2).

We find from our fitting that there is no evidence for relative motion between any of the components A1, A3, B1, B2, B4, C1 and C2 (we will refer to these components as the ‘stationary’ group). In contrast the most significant separation we find is between the outer components A2 and C2. From linear regression analysis of MODELFIT data we find a separation rate between these two components of  $14.116 \pm 1.606 \mu\text{as yr}^{-1}$  (see Fig. 3). These components are well separated on our CLEAN images

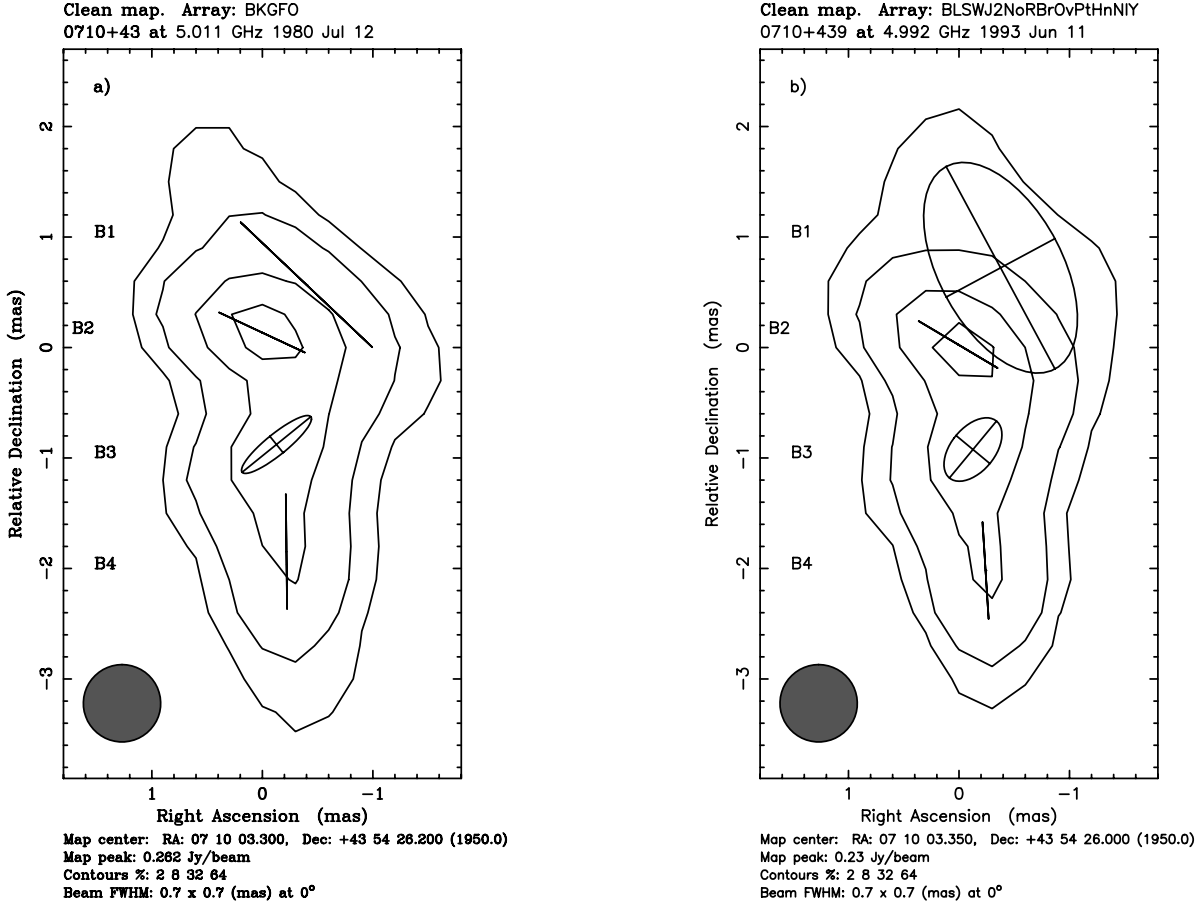


**Fig. 2a and b.** Modelfit gaussians within middle component of 0710+439 at 5 GHz convolved with a 0.7 mas restoring beam: **a** First epoch, **b** Fifth epoch

which allows us to also use the AIPS task JMFIT to fit the position of A2 and C2 on the CLEAN images at each epoch, giving a similar separation rate of  $15.538 \pm 0.445 \mu\text{as yr}^{-1}$ .

Given the small number of degrees of freedom tests of significance are best made from examining the correlation coefficients obtained from our linear regression analysis. For the MODELFIT and JMFIT analysis of the A2-C2 separation we obtain correlation coefficients between epoch and separation of 0.981 and 0.998 respectively, which allows us to reject the null hypothesis of no motion at better than the 1% and 0.1% confidence levels. Analysis of other pairs of components (see Table 3) suggests that the significant change in A2-C2 separation is caused primarily by motion of A2 northward rather than motion of C2 southward. For instance we found the separation rate of A2-B2 to be  $12.913 \pm 2.555 \mu\text{as yr}^{-1}$ , very similar to the A2-C2 separation rate. In contrast the B2-C2 separation rate of  $1.370 \pm 3.383 \mu\text{as yr}^{-1}$  is consistent with zero.

Amongst the other components the only other indication of motion is that B3 is moving northward relative to B2 (and B4 and other members of the stationary group) at a rate of  $6.089 \pm 1.752 \mu\text{as yr}^{-1}$ . We also searched for motions between component pairs in directions perpendicular to the vectors separating them but found no significant motions.

**Table 3.** Measured apparent motions of the gaussian components within 0710+439

Components	Apparent velocity [ $h^{-1}c$ ]	Estimated $1\sigma$ error [ $h^{-1}c$ ]
A2-A1	0.178	0.217
A2-A3	0.167	0.057
A2-B2	0.230	0.053
A2-B4	0.258	0.112
A2-C2	0.251	0.029
B2-B1	0.194	0.160
B2-B3	-0.107	0.032
B2-B4	0.032	0.068
B2-C2	0.025	0.061
C1-C2	-0.353	0.253

Finally in our analysis of the multi-epoch data we searched for variations in component flux densities. In order to eliminate the effects of errors on the overall flux density scale at each epoch we measured the ratio of each component's flux density to that of component C2. None of the 'stationary' components

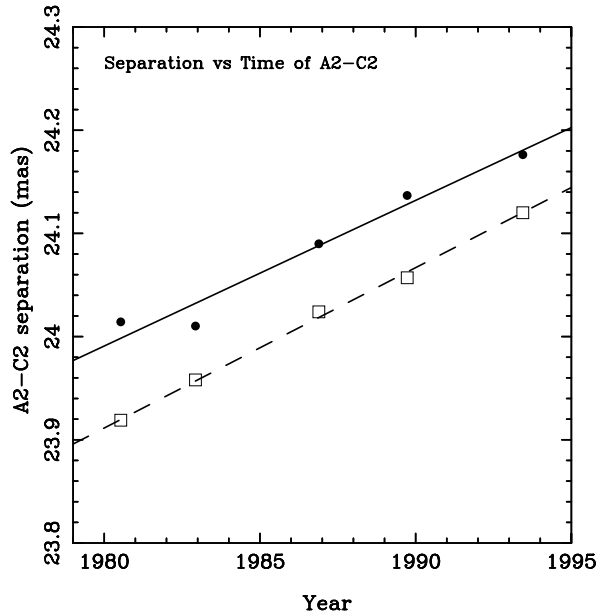


**Fig. 3.** Changes in separation with time of the components A2 and C2. Filled circles represent data obtained by MODELFIT, solid line shows linear regression fit to these data. Open squares represent data obtained by JMFIT, dashed line shows linear regression fit. See Sect. 4.2 for a discussion of the errors on the plotted points and the fits

showed significant flux variations relative to each other or to C2, strongly arguing that all these components stayed constant in flux density over the observing period. We did however detect strong variability of the flux ratio for A2/C2 (see Fig. 4), implying changes in the A2 flux density and also a possible steady increase in the flux density of B3 of about  $24\% \pm 8\%$  between the first and the last epochs.

#### 4.3. Bulk motion or internal structure changes?

The change in separation of the outer components of 0710+439 over 13 years is approximately 1/7 of the beam FWHM in the North-South direction. However we note that this shift is 1/3 of the FWHM of the A2 component in the same direction. This large shift combined with the fact that it appears to be consistent from epoch to epoch (see Fig. 3) and is the same when measured relative to several gaussian components, strongly argues that the motion of component A2 is real.

One possibility that must be eliminated is that the apparent change in the centroid position of A2 is not due to motion of the whole component northward but instead is due to changes in its internal structure. There could for instance be changes in the relative flux densities of stationary subcomponents within A2. However the non-monotonic change of the total flux density of A2 (see Fig. 4) seems to be inconsistent with a linear change of the centroid position of A2 (see Fig. 3). It also seems unlikely that if there were two subcomponents within A2 separated by a large enough distance to explain the detected centroid shift that we could still get a good fit at every epoch with a single gaussian component. Furthermore we would expect to see changes in

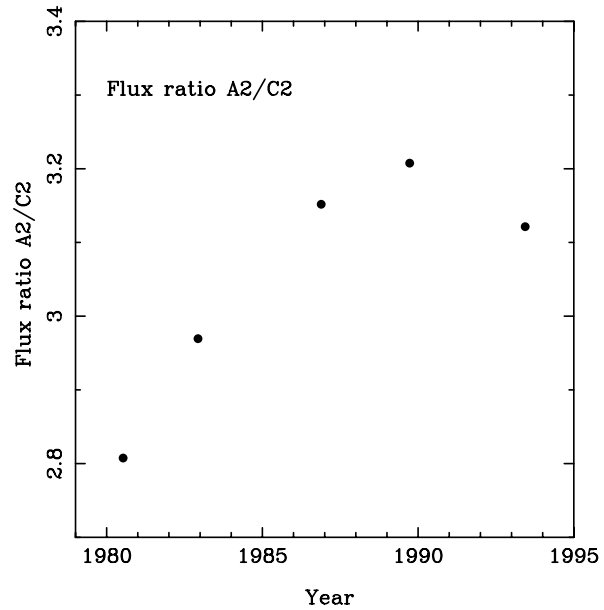


**Fig. 4.** Measurements of the flux density ratio of A2 and C2 components as a function of time

the apparent size of the component with epoch which we do not see. Another possibility is that A2 consists internally of a true stationary hotspot and a jet knot which moves toward it. Again in this case we would have difficulty fitting A2 with a single gaussian and would expect to see the width of the whole component becoming smaller with time, which we do not see. While it is always possible to construct ‘Christmas Tree’ models in which the brightening and dimming of stationary components mimics bulk motion (Scheuer 1984), such models would need to be contrived to fit the observed changes in 0710+439. We argue that the changes seen are instead due to bulk motion of A2.

#### 4.4. Motions relative to the core

Our analysis of the component motions showed (see Sect. 4.2) a group of components (A1, A3, B2, B4, C1, C2) which are stationary relative to each other. Because we were not able to detect the core position in our maps or models (except tentatively in the 5th epoch, see Sect. 3.3), we do not know for certain the motion, if any, of these components relative to the core. Despite this it seems most likely that this group is stationary relative to the core and defines a rest frame. If this is not the case then all these components, on different sides of the source, must move in unison, in a coordinated way relative to the core; a situation which appears very unlikely. Consider for instance if component C2 and hence the rest of the stationary group moves southward from the core at  $0.126 h^{-1}c$  (exactly half of the A2-C2 separation rate). This scenario has the advantage that both A2 and C2 components are then advancing away from the core at the same speed. But in this case features B2 and B4 would be moving southward *towards* the core at  $0.126 h^{-1}c$ . Since we believe that B2 and B4 are jet features the probability that both

would be moving inward toward the core at the same speed, with an amplitude exactly matching the advance speed of A2 and C2 outward, would seem to be very low. The stationary group of components might conceivably move northward, but then component C2 would be moving inwards to the core, which seems to be unphysical if C2 is, as we expect, the southern hotspot.

We conclude that the most likely scenario is that all the components in the ‘stationary group’ are also stationary with respect to the core as well as with respect to each other. In this case B2 and B4 are naturally interpreted as stationary shocks within the jet, and B3 as a possible travelling shock moving outward along the jet at  $0.1h^{-1}c$  (see Sect. 4.2). However a consequence of this model is that the advance speeds of the two outer components, A2 and C2 through the surrounding medium are likely to be different. Consider the separation rates of A2-B2 and C2-B2, which give the lowest estimated errors (see Table 3) of A2 and C2 motion relative to a stationary component. From these measurements we estimate an advance speed for A2 of  $0.230 \pm 0.053h^{-1}c$  and for C2 of  $0.025 \pm 0.061h^{-1}c$ . If jet component B2 has after all a small undetected velocity outward relative to the core then the implied asymmetry in the advance speeds of A2 and C2 relative to the core would be increased. We note however that despite the apparent velocity difference statistical tests can only exclude the null hypothesis of no difference between the A2-B2 and C2-B2 advance speeds at the 10% confidence level; this result must therefore be confirmed by future observations.

## 5. Discussion

### 5.1. Hotspot advance speeds and source age

The fact that the A2 and C2 gaussian components are compact and lie at the leading edges of the minilobe emission regions strongly argues that they should be interpreted as hotspots where two oppositely directed jets terminate (see Fig. 1a,b). In Sect. 4.2 we considered the relative separation rates of the different components of 0710+439, and found the highest significance detection to be that of the apparent separation rate of A2-C2 at  $0.251 \pm 0.029h^{-1}c$ . Since CSOs are dominated by unbeamed emission we expect for a sample selected on total flux density that the angle between the jet axis and the sky plane is about  $30^\circ$ . Such an orientation for 0710+439 is compatible with the hotspots appearing at the extreme ends of the radio emission and not superimposed on the diffuse minilobe, and is also consistent with a hotspot-core arm-length ratio which is close to one (Readhead et al 1996c). Given such an orientation we expect that the average of the two hotspot advance speeds through the external medium should be only slightly larger than that estimated from the observed separation rate (i.e. approximately  $0.126h^{-1}c$ ).

Of prime astrophysical importance is the estimated age of 0710+439. A simple estimate based on dividing the overall projected size of 0710+439 by the measured projected hotspot separation rate gives  $1100 \pm 100$  yrs, implying that 0710+439 is

a very young radio source. In assessing the reliability of this estimate we must be aware that what have actually measured (see Sect. 4.2) is the instantaneous rate of separation of the two hotspots at the present epoch; not directly the mean rate of increase of size of the whole source. Since hotspots are nearly always observed, as in 0710+439, to lie close to the ends of the lobes in which they are embedded the mean expansion speed of the whole source must equal the mean separation rate of the hotspots. However there are several mechanisms which would cause the *instantaneous* hotspot advance speeds to vary about their mean values. Variations in the external density due to encounters with clouds is one obvious mechanism. Another possibility is the so-called ‘dentist’s drill’ phenomena (Scheuer 1982) in which the position of hotspot’s working surface moves around either due to jet precession initiated at the central engine or hydrodynamic instabilities acting on the incoming jet. In this model the hotspot executes a corkscrew like-path in space and the mean rate of advance is significantly smaller than the total instantaneous speed of the hotspot. Related effects show up in recent three-dimensional numerical jet simulations (Norman 1996). These simulations also show variations in hotspot pressures and hence advance speed due to the effects of vortex shedding and cocoon turbulence acting on the incoming jet which in turn effect the jet collimation and the area over which the thrust of the jet is deposited. Due to such effects the simulations predict that instantaneous forward hotspot advance speeds (i.e. in the direction of the jet axis) can vary by factors of order two (Norman 1996).

Whatever the physical mechanism that is acting there is empirical evidence that in 0710+439 instantaneous and mean hotspot speeds are different. In 0710+439 as in other CSOs the distances from the two hotspots to the core are very similar, i.e. the ratio of these distances (the ‘arm length ratio’) is only 0.95 (Readhead et al. 1996c) which implies the mean advance speeds of the two hotspots have been the same averaged over the history of the source. In contrast as discussed in Sect 4.4, it is probable that the present instantaneous advance speeds for A2 and C2 are different from each other. Below we discuss which of the possible mechanisms is operating in 0710+439 and its impact on our age estimate.

The simplest explanation for the instantaneous speed variations is that C2 is presently interacting with a dense cloud while A2 advances rapidly through an intercloud medium. If around 100 such clouds have been encountered by each hotspot there would be enough cloud encounters to explain why the arm length ratio is close to unity, yet few enough to explain the constant velocity of A2 over 13 years. If cloud collisions were the reason for hotspot speed variations then our best estimate for the source age would depend inversely on the fraction of time,  $f$ , the hotspots spent transversing the intercloud medium. We can argue that since we apparently detect such an advance in the first CSO for which we have more than a decade of monitoring  $f$  is unlikely to be less than 0.1, and so we obtain an upper age limit of 11 000 yrs. Arguing against such a cloud mechanism operating is the expectation that if C2 were embedded within a dense cloud one might reasonably expect its pressure to *in-*

*crease* in response to the higher density, in fact we observe that the pressure in C2 is less than in A2. In addition we believe it is unlikely (although still possible) that the 'dentist's drill' effect is a significant cause of the apparent speed variations since as we discuss in Sect 4.1. the change in the apparent A2-C2 vector is mainly in its length and not its orientation. Except for certain unlikely orientations of the source and its hotspots in space one would expect hotspots effected by the dentist drill phenomena to show significant side-to-side motions.

Our favoured explanation for hotspot speed differences in 0710+439 is that these are simply related to differences in pressures of the hotspots and hence in the corresponding ram pressure velocities through a smooth external medium. Such pressure variations and resulting speed variations are as we have noted predicted by recent three-dimensional numerical simulations (Norman 1996). Assuming that A2 is close to its equipartition pressure (supported by the analysis of the frequency of its Synchrotron Self Absorbed turnover, Conway et al. 1992) and that the source is orientated not too far from the sky plane then ram pressure arguments imply an external density of  $1.83 h^{18/7} \text{ cm}^{-3}$ . This value is similar to that estimated in the CSO 2352+495 ( $3 - 10 \text{ cm}^{-3}$ , Readhead et al. 1996a) and is consistent with what is expected for the NLR intercloud medium. The data are consistent with C2 having the same external density as A2 and a lower advance speed simply as a consequence of its lower pressure. Since the equipartition pressure of C2 is 0.3 of A2, the expected advance speed for the same external density is 0.55 of A2, given the A2-C2 separation rate this implies a C2 advance speed of  $0.089 \pm 0.010 h^{-1} c$ , which is within  $1\sigma$  of the observed B2-C2 separation rate of  $0.025 \pm 0.061 h^{-1} c$ . If hotspot pressure variations are the cause of the hotspot speed variations then the observed differences in pressure between the two hotspots within individual CSOs of between 4 and 6 (see Readhead et al 1996b) imply, assuming the same external densities around each hotspot, that hotspot speed variations vary over a factor of about two within each source. We therefore expect ratios between instantaneous and mean separation rates to be of the same order and hence estimate an upper limit to the age of 0710+439 of approximately 3000yrs.

Given our age estimates and estimates of the jet thrust (Readhead et al. 1996a) we can compare the mechanical luminosity required to drive the hot spots forward with the radio luminosity and jet power. For an age of 1100yrs the combined mechanical luminosity of the two hotspots is  $0.8 \times 10^{44} h^{-17/7} \text{ erg s}^{-1}$ , while the radio luminosity of the two hotspots is about  $0.5 \times 10^{44} h^{-2} \text{ erg s}^{-1}$ . Following the arguments used in Readhead et al. (1996a) from the measured hotspot sizes and pressures the upper limit on the total power supplied by the jets is  $8.0 \times 10^{44} h^{-10/7} \text{ erg s}^{-1}$ . A lower limit on the total jet power can be obtained by adding together the radio power and mechanical work. The total jet luminosity is (for  $h=0.6$ ) therefore in the range  $4.5 \times 10^{44} \text{ erg s}^{-1}$  to  $16.6 \times 10^{44} \text{ erg s}^{-1}$  and the efficiency of conversion of jet energy to radio emission is between 8% and 31%. In contrast for classical FR II (Fanaroff & Riley 1974) radio galaxies we estimate upper limits on hotspot radiative efficiencies of a few percent by comparing total ra-

dio luminosities to estimates of the jet luminosities given by Rawlings & Sanders (1991).

## 5.2. Implications for CSO models

Our best estimate for the mean hotspot advance speed in 0710+439, given our observations, i.e  $0.13 h^{-1} c$ , is somewhat larger than that estimated by other authors for the CSO population in general (e.g. Readhead et al. 1996b estimates  $0.02c$ ). If hotspot pressures and hence advance speeds vary with time it might be that the true mean advance speeds in 0710+439 are up to a factor of two less than our best estimate (see Sect. 5.1) but a difference between predictions and observations still remains. One possibility, given that one would expect a range in properties from CSO to CSO, is that 0710+439 lies at the extreme end of the population and is growing faster than the typical CSO. However, Conway et al. (1994) tentatively detected, based on two global 5 GHz epochs, mean hotspot advance velocities of  $0.09 h^{-1} c$  in another CSO, 0108+388. A similar rate of advance was also detected by Taylor et al (1996) in the same source. Recently a mean hotspot advance speed of  $0.098 \pm 0.013 h^{-1} c$  has been confirmed in 0108+388 by three epoch global 5 GHz observations (Owsianik et al. 1998). Conway et al. (1994) also detected a hotspot advance speed of  $0.065 h^{-1} c$  in the object 2021+614 which may also be a CSO. Finally for the CSO 2352+495 Readhead et al. (1996a) gives age estimates of 1200 - 1800 yrs based on synchrotron ageing and 1500 - 7500 yrs from energy supply arguments. For this source of size  $120 h^{-1} \text{ pc}$  an age near the lower end of the allowed range, i.e. 1500 yrs gives a mean hotspot advance speed of  $0.13 h^{-1} c$ .

The lower estimate of hotspot advance speeds for the CSO population in general ( $0.02c$ ) made by Readhead et al. (1996a) was based on a two part argument, namely: i) it was argued that hotspot pressures adjusted to the external density so that hotspot advance speeds are constant. Therefore advance speeds of high pressure hotspots in young sources transversing the dense ISM are the same as in the classical double sources; ii) Classical double sources, based primarily on observations of Cygnus A, have advance speeds of  $0.02c$ .

The first part of the above argument was based on detailed observations of three CSOs, in which the arm-length ratios are close to one and therefore the mean advance speeds for the two hotspots must be the same, despite in each case the pressures of the two hotspots being quite different. Readhead et al. (1996b) explicitly assumed that the characteristics of the hotspots are constant in time and that the pressure ratios measured now are typical of the whole history of these sources. It follows that hotspot advance speeds must be independent of hotspot pressure. It was postulated that this could be achieved if a mechanism existed where the hotspot pressure always adjusted to the external density so that ram pressure balance gave a constant advance speed.

In contrast 3-D numerical simulations (Norman 1996) indicate that due to hydrodynamic effects individual hotspots can rapidly vary their pressures around some mean value as they move outward, with corresponding variations in their

ram-pressure advance speeds. Differences in pressures between hotspots seen in maps may therefore be just temporary features of sources. Arm length ratios close to one are simply explained if external densities and mean hotspot pressures on each side of the source are the same, so that mean advance speeds are the same. It follows that no special mechanism is required which adjusts hotspot pressure to external density in order to explain the observations. The main motivation which led Readhead et al. (1996b) to propose a universal constant hotspot advance speed for both CSOs and classical sources is therefore removed.

In contrast to Readhead et al.'s (1996b) observational approach Begelman (1996) has calculated the evolution expected for a simple theoretical model of a source with an overpressurised cocoon and a hotspot whose mean pressure is a fixed ratio to that of the cocoon. In this model the advance speed depends on the density versus distance of the external medium  $\rho \propto r^{-n}$ , such that the advance speed  $v_h \propto l^\beta$  where  $l$  is the source size and  $\beta = (n - 2)/3$ . For  $n$  in the plausible range 1.5 to 2.0, then  $\beta$  is in the range  $-0.17$  to  $0.0$ . It is therefore possible that hotspot advance speeds in CSOs are somewhat faster than in classical sources. Since CSOs are 1000 times smaller than classical sources if  $n$  were 1.5, we expect advance speeds which are about 3 times faster.

Readhead et al. (1996a) estimated advance speeds in classical sources to be  $0.02c$ , mainly based on Cygnus A results. However it appears that Cygnus A is an unusual source in that it lies in an unusually dense environment (Barthel & Arnaud 1996, Reynolds & Fabian 1996). In other FRII's external densities are estimated to be 30 times smaller (Rawlings & Saunders 1991) yet hotspot pressures are only 3 times smaller (Readhead et al. 1996b), implying that typical ram pressure advance speeds in classical sources might be closer to  $0.06c$ . Hotspot advance speeds can also be estimated independently from electron spectral ageing arguments and from arm-length asymmetries in classical double sources. Using the first method the data of Rawlings & Saunders (1991) indicate advance speeds of  $0.108 \pm 0.098 h^{-4/7} c$ ; other studies indicate velocities which are greater than  $0.1c$  (e.g. Liu et al. 1992). Such estimates might however be larger than the real advance speeds since strictly speaking they measure the sum of the advance speed of the hotspot and the speed of the backflow from it (see Liu et al. 1992 and Scheuer 1995). This would be consistent with the fact that for the same sample of sources observations of jet/counter-jet side arm length ratios indicate (Scheuer 1995) smaller advance speeds of  $0.03 \pm 0.02c$ . The present data on hotspot advance speeds does not yet yield a definite conclusion but certainly allows the possibility that these speeds could be a factor of three larger than estimated by Readhead et al. (1996a).

Combining a typical FRII advance speed of say  $0.06c$  with the probable weak evolution of hotspot advance speeds with source size we find that mean hotspot advance speeds in CSOs can plausibly be  $0.2c$  or larger. We conclude that the size of the measured hotspot speed in 0710+439 is compatible with the predictions of theoretical models. Such fast speeds imply that sources have only a short lifetime in the CSO phase. The fact that up to 10% of sources in flux limited samples at 5 GHz are CSOs

therefore means either that i) not all CSOs evolve into classical sources; some exhaust their fuel before reaching 100kpc size (Readhead et al. 1994) or ii) there is strong luminosity evolution in their radio emission. We favour the second explanation, strong luminosity evolution of the required amount to explain the source size distribution is in fact predicted by the theoretical models. For instance the Begelman (1996) model predicts a radio luminosity proportional to approximately  $l^{-0.5}$  assuming a constant jet mechanical power. For the weakly evolving hotspot advance velocity predicted for an external density of the form  $\rho \propto r^{-1.5}$ , the predicted number of sources in each decade of size then exactly matches the observations (Begelman 1996). As first noted by Readhead et al. (1996a) for 2352+495, and as we find for 0710+439 (see Sect. 5.1), the limits on the radiative efficiency for CSOs compared to classical sources empirically demonstrate that the expected luminosity evolution does in fact occur and with a magnitude (a factor of 30 from CSO to classical sources) consistent with that expected by theory. Given this efficiency evolution one would expect 0710+439 to evolve into a source of radio luminosity  $L_{178MHz} = 8 \times 10^{25} h^{-2} W Hz^{-1}$ , i.e. a weak FRII. We conclude that CSOs are probably very young extragalactic radio sources and that furthermore they probably evolve into lower luminosity FRII classical double radio sources.

*Acknowledgements.* We thank the observatories of the US and European VLBI Networks and NRAO, which operates the VLA and the VLBA. NRAO is operated by Associated Universities, Inc., under cooperative agreement with the National Science Foundation. I. Owsianik acknowledges support from the Polish State Committee for Scientific Research grant nr 2.P304.003.07, EU grant (ERBCIPDCT940087) and Onsala Space Observatory. We thank the referee for his helpful comments. We thank G.B. Taylor for helping schedule the 1993 observations.

## Appendix

We must be careful with the interpretation of multi-epoch data, because analysis methods can strongly affect the reliability of our results. It is very important to know which features to believe, and how accurate our measurements of very small changes are. To investigate these problems we made mapping and model-fitting tests in which we generated simulated data using the program FAKE in the Caltech VLBI data analysis package with the same  $u-v$  coverages as the real observations. These 'fake' data contained realistic additive Gaussian noise, random antenna-based phase errors and time-varying amplitude calibration errors of order of 10%.

### A.1. Reliability of features in CLEAN maps

Fake data for the 1st and 5th epoch were made using the same 9 gaussian components model, which was fitted to the real 5th epoch data (see Table 2). These simulated data were each mapped separately with a point component as a starting model. The final maps had different extended structures in the northern and southern components, they also contained apparent bridge

emission between these three main components, which was not part of the model. These detected errors were presumably due to inadequacies and differences in  $u$ - $v$  coverage at each epoch combined with differences in the details of mapping at each ‘fake’ epoch (choice of windows etc). This test leads us to the conclusion that the details of diffuse and bridge structures seen in the CLEAN maps made from the real data (see Fig. 1a) are not reliable. We also conclude that using maps made separately at each epoch is an unreliable way of detecting changes in source structure.

### A.2. Estimating modelfitting component position errors

As described in Sect. 4.1 we can set accurate limits on component motions by gaussian modelfitting to each epoch. We carried out ‘fake’ simulations to answer two questions about this procedure. The first was to determine the size of the remaining random errors due to different  $u$ - $v$  coverages and data reduction at each epoch under the null hypothesis of no component motion. The second question was to investigate if this method introduced systematic errors by biasing the results in the sense that real changes would be removed or reduced by initially trying to force the data at each epoch to agree with the same 5th epoch starting model.

In our first test in order to make the simulation as realistic as possible we attempted to take account of the fact that the real source structure in 0710+439 is almost certainly more complex than can be represented by 9 Gaussian components. This complexity is demonstrated by the fact the final agreement factors (see Sect. 4.1) of our models are further from unity than would be expected purely from random noise. It is conceivable that this extra complexity might interact with differences in  $u$ - $v$  coverage to give apparent changes in the centroid position when a 9 component model is fitted at each epoch, even if no position changes actually occur in the source. To test the above possibility we created a 18 component model by replacing each component in the original 9 component model by two slightly shifted gaussians. The final model was such that the agreement factors on fitting a 9 component model to the corresponding ‘fake’ data was roughly similar to that obtained with the real data.

Having chosen a suitable 18 component model we created ‘fake’ data for the 1st and 5th epochs. Using a procedure as similar as possible to that used to analyse the real data we then fitted a 9 component model at each epoch and compared the separations between the gaussians we obtained. The size of the apparent changes gave us an estimate of the residual random error. On doing this test we found an apparent change of A2-C2 separation of  $8.09 \mu\text{as}$  and in the A2-B2 separation of  $30.9 \mu\text{as}$  between the 1st and the 5th epochs. The values are much smaller than the changes in component separation which we detected from the real data (see Fig. 3) and comparable with the variances we estimated from linear regression analysis (see Sect. 4.2).

### A.3. Biasing due to cross self-calibration

In our final test we sought to determine if our modelfitting procedure introduced a systematic error due to initially self-calibrating all models against the same 5th epoch starting model. It is possible that real changes might be reduced or removed by initially trying to force all epochs to agree with the 5th epoch model. To quantify this effect we simulated the case of a  $200 \mu\text{as}$  shift of A2 (and then C2) position between epochs 1 and 5. Applying our standard modelfitting procedure (see Sect. 4.1) we determined an estimated motion of just under  $200 \mu\text{as}$ . The largest negative bias found in our test was only  $9 \mu\text{as}$ . We conclude that this biasing mechanism has a negligible effect on the estimate in the shift of A2 seen in the real data.

## References

- Aller M.F., Aller H.D., Hughes P.A., 1992, ApJ 399, 16  
 Barthel P.D., Arnaud K.A., 1996, MNRAS 283, L45  
 Begelman M.C., 1996, Baby Cygnus A's. In: Carilli C.L., Harris D.E. (eds.) Proc. of the Greenbank Workshop, Cygnus A-study of a Radio Galaxy. CUP, Cambridge, p.209  
 Clark B.G., 1973, Proc IEEE, 61, 1242  
 Conway J.E., Pearson T.J., Readhead A.C.S., et al., 1992, ApJ 396, 62  
 Conway J.E., Myers S.T., Pearson T.J., et al., 1994, ApJ 425, 568  
 Fanaroff B.L., Riley J.M., 1974, MNRAS 167, 31  
 Fanti C., Fanti R., Dallacasa D. et al., 1995, A & A 302, 317  
 Henstock D.R., Browne I.W.A., Wilkinson P.N., et al., 1995, ApJS 100, 1  
 Lawrence C.R., Zucker J.R., Readhead A.C.S., et al., 1996, ApJS 107, 541  
 Liu R., Pooley G., Riley J.M., 1992, MNRAS 257, 545  
 Norman M.L., 1996, Structure and Dynamics of the 3D Supersonic Jet. In: Hardee P.E., Bridle A.H., Zensus J.A. (eds.) Energy Transport in Radio Galaxies and Quasars. ASP, San Francisco, vol.100, p.319  
 O'Dea, C.P., 1998, PASP, in press  
 Owsianik I., Conway J.E., Polatidis A.G., 1998, A&A, accepted  
 Peacock J.A., Perryman M.A.C., Longair M.S., Gunn J.E., Westphal J.A., 1981, MNRAS 194, 601  
 Pearson T.J., 1991, BAAS 23, 991  
 Pearson T.J., Readhead A.C.S., 1988, ApJ 328, 114  
 Phillips R.B., Mutel R.L., 1982, A & A 106, 21  
 Rawlings S., Saunders R., 1991, Nat 349, 138  
 Readhead A.C.S., Xu W., Pearson T.J., Wilkinson P.N., Polatidis A.G., 1994, Compact Symmetric Objects. In: Zensus J.A., Kellermann K.I. (eds.) Proc. of NRAO Workshop No.23, Compact Extragalactic Radio Source. NRAO, p.17  
 Readhead A.C.S., Taylor G.B., Xu W., et al., 1996a, ApJ 460, 612  
 Readhead A.C.S., Taylor G.B., Pearson T.J., Wilkinson P.N., 1996b, ApJ 460, 634  
 Readhead A.C.S., Pearson T.J., Taylor G.B., Wilkinson P.N., 1996c, The Jet Advance Speed in Compact Symmetric Objects. In: Hardee P.E., Bridle A.H., Zensus J.A. (eds.) Energy Transport in Radio Galaxies and Quasars. ASP, San Francisco, vol.100, p.79  
 Reynolds C.S., Fabian A.C., 1996, MNRAS 278, 479  
 Scheuer P.A.G., 1982, Morphology and power of radio sources. In: Heeschen D.S., Wade C.M. (eds.) Proc. IAU Symp. 97, Extragalactic Radio Source. Reidel, Dordrecht, p.163  
 Scheuer P.A.G., 1984, Explanations of Superluminal motion. In: Fanti R., Kellermann K., and Setti G. (eds.) Proc. IAU Symp. 110, VLBI and Compact Radio Sources. Reidel, Dordrecht, p.197

- Scheuer P.A.G., 1995, MNRAS 277, 331  
Schwab F.R., Cotton W.D., 1983, AJ 88, 688  
Shepherd M.C., Pearson T.J., Taylor G.B., 1995, BAAS 27, 903  
Taylor G.B., Readhead A.C.S., Pearson T.J., 1996, ApJ 463, 95  
Wilkinson P.N., Polatidis A.G., Readhead A.C.S., Xu W., Pearson T.J.,  
1994, ApJ 432, L87  
van Breugel W., Miley G., Heckman T., 1984, AJ 89, 5  
Xu W., 1994, Ph.D. Thesis, California Institute of Technology  
de Young D.S., 1996, How do CSO's Grow Old? In: Snellen I.A.G.,  
Schilizzi R.T., Röttgering M.J.A., Bremer M.N. (eds.) The Sec-  
ond Workshop on Gigahertz Peaked Spectrum and Compact Steep  
Spectrum Radio Sources. Leiden Observatory, Leiden, p.275